



Evidence for the two-body charmless baryonic decay $B^+ \rightarrow p\bar{\Lambda}$

The LHCb collaboration[†]

Abstract

A search for the rare two-body charmless baryonic decay $B^+ \rightarrow p\bar{\Lambda}$ is performed with pp collision data, corresponding to an integrated luminosity of 3 fb^{-1} , collected by the LHCb experiment at centre-of-mass energies of 7 and 8 TeV. An excess of $B^+ \rightarrow p\bar{\Lambda}$ candidates with respect to background expectations is seen with a statistical significance of 4.1 standard deviations, and constitutes the first evidence for this decay. The branching fraction, measured using the $B^+ \rightarrow K_S^0 \pi^+$ decay for normalisation, is

$$\mathcal{B}(B^+ \rightarrow p\bar{\Lambda}) = (2.4_{-0.8}^{+1.0} \pm 0.3) \times 10^{-7},$$

where the first uncertainty is statistical and the second systematic.

Published in JHEP 04 (2017) 162

© CERN on behalf of the LHCb collaboration, licence CC-BY-4.0.

[†]Authors are listed at the end of this paper.

1 Introduction

The experimental study of B meson decays to baryonic final states has a long history, including numerous searches and observations by the asymmetric e^+e^- collider experiments BaBar and Belle [1]. In recent years the LHCb collaboration reported the first observation of a two-body charmless baryonic B^+ decay and the first evidence for a similar B^0 decay, namely $B^+ \rightarrow p\bar{\Lambda}(1520)$ [2] and $B^0 \rightarrow p\bar{p}$ [3]. No other two-body charmless baryonic B decay modes have been observed. Their experimental study requires large data samples, presently only available at the LHC, as baryonic B decays to two-body final states are suppressed, with branching fractions typically one to two orders of magnitude lower than similar baryonic decays to multibody final states.

Experimental input on the branching fractions of the $B^+ \rightarrow p\bar{\Lambda}$ decay and other suppressed baryonic decays provides valuable information on the dynamics of the decays of B mesons to baryonic final states. The $B^+ \rightarrow p\bar{\Lambda}$ decay mode is expected to be dominated by a $b \rightarrow s$ loop transition, but tree-level (V_{ub} suppressed) and annihilation diagrams also contribute. Various theoretical predictions for its branching fraction are available. Calculations based on QCD sum rules [4] predict a branching fraction smaller than 3×10^{-6} whereas a pole model [5] and a recent study [6], taking into account the LHCb experimental result on the $B^0 \rightarrow p\bar{p}$ branching fraction [3], both predict a branching fraction around 2×10^{-7} . The violation of partial conservation of the axial-vector current at the GeV scale has been proposed as an alternative approach to the understanding of the data available on two-body baryonic decays of B and D_s^+ mesons [7]. It explains the LHCb results on the $B_{(s)}^0 \rightarrow p\bar{p}$ decay modes [3] and predicts a branching fraction for the $B^+ \rightarrow p\bar{\Lambda}$ decay of the order of 10^{-8} .

The decay $B^+ \rightarrow p\bar{\Lambda}$ has been searched for by the CLEO [8] and Belle [9] collaborations. The most stringent experimental upper limit on the $B^+ \rightarrow p\bar{\Lambda}$ branching fraction is 3.2×10^{-7} at 90% confidence level, determined by the Belle collaboration using 414 fb^{-1} of integrated luminosity from e^+e^- collisions.

This paper presents a search for the rare decay mode $B^+ \rightarrow p\bar{\Lambda}$ with the full pp collision data sample collected in 2011 and 2012 by the LHCb experiment. The branching fraction is measured with respect to that of the topologically identical $B^+ \rightarrow K_s^0\pi^+$ decay to suppress common systematic uncertainties. The Λ baryon is reconstructed in the $\Lambda \rightarrow p\pi^-$ final state whereas the K_s^0 meson is reconstructed in its $K_s^0 \rightarrow \pi^+\pi^-$ final state. The inclusion of charge-conjugate processes is implied throughout this paper.

2 Detector and data sample

The data sample analysed corresponds to an integrated luminosity of 1 fb^{-1} at a centre-of-mass energy of 7 TeV recorded in 2011 and 2 fb^{-1} at 8 TeV recorded in 2012. The LHCb detector [10, 11] is a single-arm forward spectrometer covering the pseudorapidity range $2 < \eta < 5$, designed for the study of particles containing b or c quarks. The detector includes a high-precision tracking system consisting of a silicon-strip vertex detector surrounding the pp interaction region, a large-area silicon-strip detector located upstream of a dipole magnet with a bending power of about 4 Tm, and three stations of silicon-strip detectors and straw drift tubes placed downstream of the magnet. The tracking system provides a measurement of momentum, p , of charged particles with

a relative uncertainty that varies from 0.5% at low momentum to 1.0% at 200 GeV/ c . The minimum distance of a track to a primary vertex (PV), the impact parameter (IP), is measured with a resolution of $(15 + 29/p_T) \mu\text{m}$, where p_T is the component of the momentum transverse to the beam, in GeV/ c . The different types of charged hadrons are distinguished using information from two ring-imaging Cherenkov detectors. Photons, electrons and hadrons are identified by a calorimeter system consisting of scintillating-pad and preshower detectors, an electromagnetic calorimeter and a hadronic calorimeter. Muons are identified by a system composed of alternating layers of iron and multiwire proportional chambers.

The decays of the V^0 hadrons, namely $\Lambda \rightarrow p\pi^-$ and $K_s^0 \rightarrow \pi^+\pi^-$, are reconstructed in two different categories: the first consists of V^0 hadrons that decay early enough for the daughter particles to be reconstructed in the vertex detector, and the second contains those that decay later such that track segments cannot be reconstructed in the vertex detector. These categories are referred to as *long* and *downstream*, respectively. The candidates in the long category have better mass, momentum and vertex resolution than those in the downstream category.

Events are selected in a similar way for both the $B^+ \rightarrow p\bar{\Lambda}$ signal decay and the normalisation channel $B^+ \rightarrow K_s^0\pi^+$. The online event selection is performed by a trigger consisting of a hardware stage, based on information from the calorimeter and muon systems, followed by a software stage that performs a full event reconstruction, in which all charged particles with $p_T > 500$ (300) MeV/ c are reconstructed for the 2011 (2012) data. At the hardware trigger stage, events are required to have a muon with high p_T or a hadron, photon or electron with high transverse energy in the calorimeters. The transverse energy threshold for hadrons is set at 3.5 GeV. Signal candidates may come from events where the hardware trigger was activated either by signal particles or by other particles in the event. The proportion of events triggered by other particles in the event is found to be very similar between the signal and the normalisation decay modes in both long and downstream samples. The software trigger requires a two- or three-track secondary vertex with a significant displacement from the primary pp interaction vertices. At least one charged particle must have $p_T > 1.7$ GeV/ c and be inconsistent with originating from a PV. A multivariate algorithm [12] is used for the identification of secondary vertices consistent with the decay of a b hadron to a final state of two or more particles.

The efficiency of the software trigger selection on both decay modes varied during the data-taking period. During the 2011 data taking, downstream tracks were not reconstructed in the software trigger. Such tracks were included in the trigger during the 2012 data taking and a further significant improvement in the algorithms was implemented mid-year. Consequently, the data are subdivided into three data-taking periods (2011, 2012a and 2012b) in addition to the two V^0 reconstruction categories (long and downstream). The 2012b sample has the highest trigger efficiency, especially in the downstream category, and is also the largest data set, corresponding to 1.4 fb^{-1} of integrated luminosity.

Simulated data samples are used to study the response of the detector and to investigate possible sources of background to the signal and the normalisation modes. The pp collisions are generated using PYTHIA [13] with a specific LHCb configuration [14]. Decays of hadronic particles are described by EVTGEN [15], in which final-state radiation is generated using PHOTOS [16]. The interaction of the generated particles with the detector, and its response, are implemented using the GEANT4 toolkit [17] as described in Ref. [18].

3 Sample selection and composition

The selection consists of two stages, a preselection with high efficiency for the signal decays, followed by a multivariate classifier. The selection requirements of both signal and normalisation decays exploit the characteristic topology and kinematic properties of two-body decays to final states containing a V^0 hadron. The B^+ candidates are reconstructed by combining, in a good-quality vertex, a V^0 candidate with a charged particle hereafter referred to as the bachelor particle. Both the $B^+ \rightarrow p\bar{\Lambda}$ and the $B^+ \rightarrow K_s^0\pi^+$ decay chains are refitted [19] using the known Λ or K_s^0 mass [20]. The resulting B^+ invariant-mass resolutions are improved and nearly identical for the long and downstream V^0 candidates. The long and downstream samples are thus merged after full selection, thereby simplifying the extraction of the signal yields.

A minimum p_T requirement is imposed for all final-state particles. The V^0 decay products must have a large IP with respect to all PVs; hence a minimum χ_{IP}^2 with respect to the PVs is imposed on each decay product, where χ_{IP}^2 is defined as the difference between the vertex-fit χ^2 of a PV reconstructed with and without the track in question. The V^0 decay products are also required to form a good quality vertex. The V^0 candidate is associated to the PV that gives the smallest χ_{IP}^2 . The selection favours long-lived V^0 decays by requiring that the decay vertex and the associated PV are well separated.

The Λ decay products must satisfy $|m(p\pi) - m_\Lambda| < 20(15) \text{ MeV}/c^2$ for downstream (long) candidates, where m_Λ is the known Λ mass [20]. The corresponding criterion for the K_s^0 decay products is $|m(\pi\pi) - m_{K_s^0}| < 30(15) \text{ MeV}/c^2$, where $m_{K_s^0}$ is the known K_s^0 mass [20].

The B^+ candidate is required to have a small χ_{IP}^2 with respect to the associated PV as its reconstructed momentum vector should point to its production vertex. This pointing condition of the B^+ candidate is further reinforced by requiring that the angle between the B^+ candidate momentum vector and the line connecting the associated PV and the B^+ decay vertex (B^+ direction angle) is close to zero.

To avoid selection biases, $p\bar{\Lambda}$ candidates with invariant mass within $64 \text{ MeV}/c^2$ (approximately four times the mass resolution) around the known B^+ mass are not examined until all analysis choices are finalised. No such procedure is applied to the spectrum of the well-known $B^+ \rightarrow K_s^0\pi^+$ decay. The final selections of $p\bar{\Lambda}$ and $K_s^0\pi^+$ candidates rely on artificial neural networks [21], multilayer perceptrons (MLPs), as multivariate classifiers to separate signal from background; the MLP implementation is provided by the TMVA toolkit [22].

Separate MLPs are employed for the $p\bar{\Lambda}$ and the $K_s^0\pi^+$ selection. The MLPs are trained with simulated samples to represent the signals and with data from the high-mass sideband in the range $5350\text{--}6420 \text{ MeV}/c^2$ for the background, to avoid partially reconstructed backgrounds. For the well-known $K_s^0\pi^+$ spectra both low- and high-mass sidebands are used. The training and selection is performed separately for each period of data taking (the 2012a and 2012b samples are merged) and for downstream and long samples. Optimisation biases are avoided by splitting each of these samples into three disjoint subsamples: each MLP is trained on a different subsample in such a way that events used to train one MLP are classified with another. The response of the MLPs is uncorrelated with the mass of the $p\bar{\Lambda}$ and $K_s^0\pi^+$ final states. The MLP training relies on an accurate description of the distributions of the input variables in simulated events. The agreement between data and simulation is verified with kinematic distributions from

$B^+ \rightarrow K_s^0 \pi^+$ decays, where the combinatorial background in the invariant mass spectrum is statistically suppressed using the *sPlot* technique [23]. No significant deviations are found, giving confidence that the inputs to the MLPs represent the data reliably. The variables used in the MLP classifiers are properties of the B^+ candidate and of the bachelor particle and V^0 daughters. The input variables are the following: the χ^2 per degree of freedom of the kinematic fit of the decay chain; the B^+ decay length, χ_{IP}^2 and direction angle; the difference between the z -positions of the B^+ and the V^0 decay vertices divided by its uncertainty squared; the bachelor particle p_{T} ; and the p_{T} of the V^0 decay products. Extra variables are exploited in the selection of the long samples: the χ_{IP}^2 of the bachelor particle and of both V^0 decay products.

In addition to the MLP selection, particle identification (PID) requirements are necessary to reject sources of background coming from B decays. A loose PID requirement is imposed on the V^0 daughters, exploiting information from the ring-imaging Cherenkov detectors, to remove background from K_s^0 (Λ) decays in the $p\bar{\Lambda}$ ($K_s^0 \pi^+$) samples. The PID selection on the bachelor particle is optimised together with the MLP selection as follows. The figure of merit $\epsilon_{\text{sig}}/(a/2 + \sqrt{B_{\text{exp}}})$ suggested in Ref. [24] is used to determine the optimal MLP and PID requirements for each $B^+ \rightarrow p\bar{\Lambda}$ subsample separately, where ϵ_{sig} represents the combined MLP and PID selection efficiency. The term $a = 3$ quantifies the target level of significance in units of standard deviations. The expected number of background candidates, B_{exp} , within the (initially excluded) signal region is estimated by extrapolating the result of a fit to the invariant mass distribution of the data sidebands. A standard significance $S/\sqrt{S+B}$ is used to optimise the selection of the $B^+ \rightarrow K_s^0 \pi^+$ candidates, where B is the number of background candidates and S the number of signal candidates in the invariant mass range $5000 - 5600 \text{ MeV}/c^2$. The presence of the cross-feed background $B^+ \rightarrow K_s^0 K^+$ is taken into account. The fraction of events with more than one selected candidate is negligible; all candidates are kept.

Efficiencies are determined for each data-taking period and each V^0 reconstruction category, and subsequently combined accounting for the mixture of these subsamples in data. The efficiency of the MLP selection is determined from simulation. Large data control samples of $D^0 \rightarrow K^- \pi^+$, $\Lambda \rightarrow p \pi^-$ and $\Lambda_c^+ \rightarrow p K^- \pi^+$ decays are employed [25] to determine the efficiency of the PID requirements. All other selection efficiencies, *i.e.* trigger, reconstruction and preselection efficiencies, are determined from simulation. The overall selection efficiencies of this analysis are of order 10^{-4} . The expected yield of the control mode $B^+ \rightarrow K_s^0 \pi^+$, calculated from the product of the integrated luminosity, the $b\bar{b}$ cross-section, the b hadronisation probability, the $B^+ \rightarrow K_s^0 \pi^+$ visible branching fraction and the total selection efficiency, agrees with the yield obtained from the fit to the data at the level of 1.4 standard deviations.

Possible sources of non-combinatorial background to the $p\bar{\Lambda}$ and $K_s^0 \pi^+$ spectra are investigated using extensive simulation samples. These sources include partially reconstructed backgrounds in which one or more particles from the decay of a b hadron are not associated with the signal candidate, and b -hadron decays where one or more decay products are misidentified, such as decays with K_s^0 mesons misidentified as Λ baryons in the $p\bar{\Lambda}$ spectrum. The peaking background from $B^+ \rightarrow p\bar{p}\pi^+$ decays in the $p\bar{\Lambda}$ spectrum is found to be insignificant after the MLP selection. The currently unobserved $B^+ \rightarrow p\bar{\Sigma}^0$ decay is treated as a source of systematic uncertainty. The ensemble of specific backgrounds does not peak in the signal region but rather contributes a smooth $p\bar{\Lambda}$ mass spectrum, which is indistinguishable from the dominant combinatorial background.

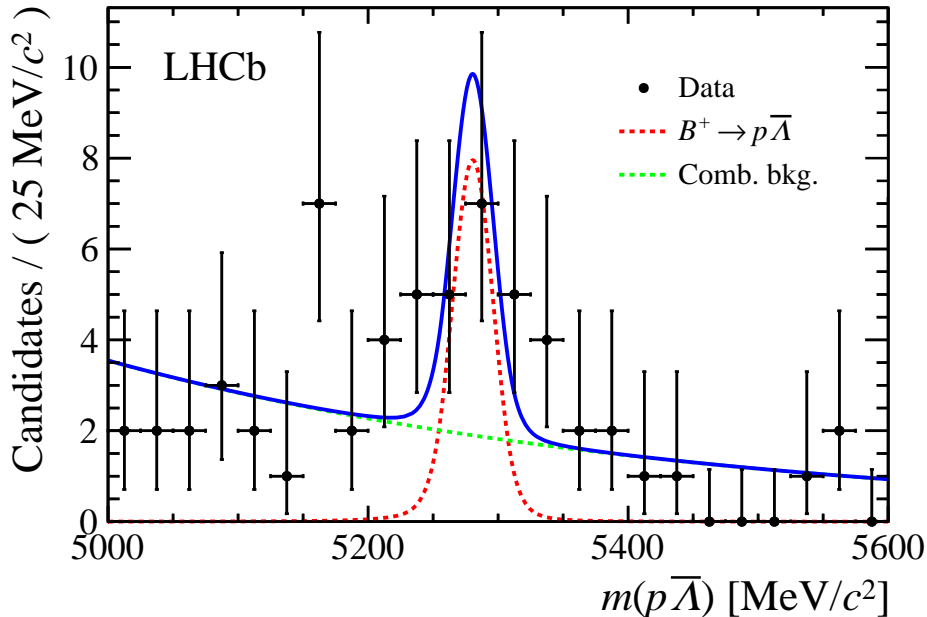


Figure 1: Invariant mass distribution of $p\bar{\Lambda}$ candidates after full selection. The result of the fit to the data (blue, solid) is shown together with each fit model component, namely the $B^+ \rightarrow p\bar{\Lambda}$ signal and the combinatorial background.

4 Signal yield determination

The yields of the signal and background candidates in both the signal and normalisation samples are determined, after the full selection, using unbinned extended maximum likelihood fits to the invariant mass spectra. The signal lineshapes are found to be compatible between the data-taking periods and between the long and downstream categories, so all subsamples are merged together into a single spectrum.

The probability density functions (PDFs) of B -meson signals have asymmetric tails that result from a combination of detector-related effects and effects of final-state radiation. The signal mass distributions are verified in simulation to be modelled accurately by the sum of two Crystal Ball (CB) functions [26] describing the high- and low-mass asymmetric tails. The peak values and the core widths of the two CB components are set to be the same.

The $p\bar{\Lambda}$ spectrum comprises the $B^+ \rightarrow p\bar{\Lambda}$ signal and combinatorial background. Contamination from partially reconstructed backgrounds, with or without misidentified particles, is treated as a source of systematic uncertainty. The peak position and tail parameters of the $B^+ \rightarrow p\bar{\Lambda}$ CB components are fixed to the values obtained from simulation. The core width parameter, also fixed, is obtained by multiplying the value from simulation by a scaling factor to account for differences in the resolution between data and simulation. This factor, determined from the $B^+ \rightarrow K_s^0 \pi^+$ data and simulation samples, is compatible with unity (1.01 ± 0.06) and gives a width of approximately $16 \text{ MeV}/c^2$. The invariant mass distribution of the combinatorial background is described by an exponential function, with the slope parameter determined from the fit.

The fit to the $p\bar{\Lambda}$ invariant mass distribution, presented in Fig. 1, determines three parameters: two yields and the slope of the combinatorial background model. An excess

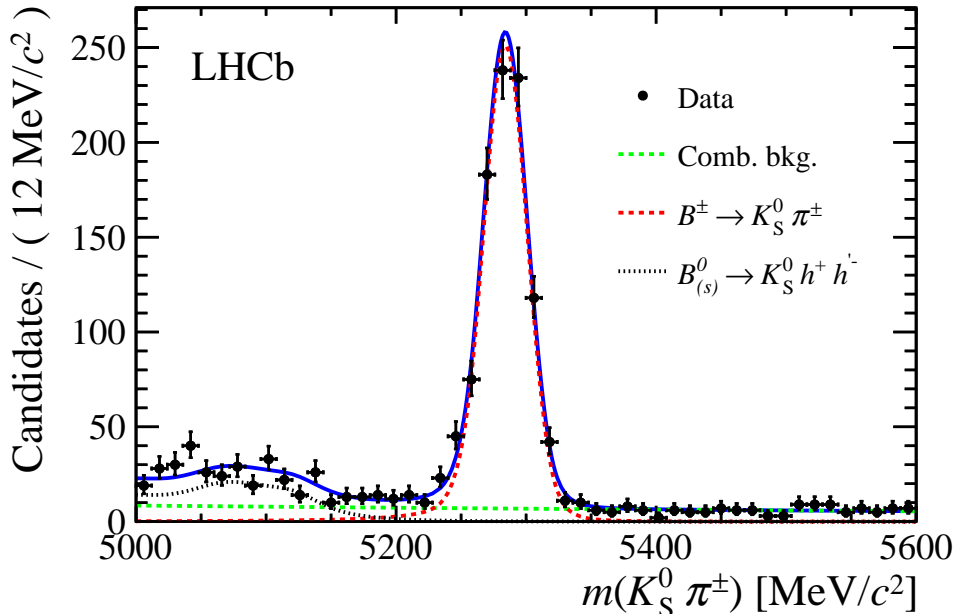


Figure 2: Invariant mass distribution of $K_S^0\pi^+$ candidates after full selection. The result of the fit to the data (blue, solid) is shown together with each fit model component, namely the $B^+ \rightarrow K_S^0\pi^+$ signal, the $B_{(s)}^0 \rightarrow K_S^0 h^+ h'^-$ partially reconstructed background, and the combinatorial background. The vanishingly small $B^+ \rightarrow K_S^0 K^+$ misidentified cross-feed is not displayed.

of $B^+ \rightarrow p\bar{\Lambda}$ candidates with respect to background expectations is found, corresponding to a signal yield of $N(B^+ \rightarrow p\bar{\Lambda}) = 13.0_{-4.3}^{+5.1}$, where the uncertainties, obtained from a profile likelihood scan, are statistical only.

The statistical significance of the $B^+ \rightarrow p\bar{\Lambda}$ signal is determined with a large set of samples simulated assuming the presence of background only. For each simulated sample, a number of events distributed according to the exponential model of the background is drawn from a Poisson distribution with mean equal to the number of observed background events. For each sample, the log-likelihood ratio $2 \ln(L_{S+B}/L_B)$ is computed, where L_{S+B} and L_B are the likelihoods from the full fit and from the fit without the signal component, respectively. The fraction of samples that yield log-likelihood ratios larger than the ratio observed in data is 3.4×10^{-5} , which corresponds to a statistical significance of 4.1 standard deviations. Inclusion of the 6.7% systematic uncertainty affecting the signal yield gives only a marginal change in the signal significance.

The $K_S^0\pi^+$ mass spectrum of the normalisation decay is described as the sum of components accounting for the $B^+ \rightarrow K_S^0\pi^+$ signal, the $B^+ \rightarrow K_S^0 K^+$ misidentified background, backgrounds from partially reconstructed $B_{(s)}^0 \rightarrow K_S^0 h^+ h'^-$ decays ($h^{(\prime)} = \pi, K$), and combinatorial background. Any contamination from other decays is treated as a source of systematic uncertainty.

The $B^+ \rightarrow K_S^0 h^+$ CB tail parameters and the relative normalisation of the two CB functions are fixed to the values obtained from simulation. The mean and the width (approximately $17 \text{ MeV}/c^2$) of the $B^+ \rightarrow K_S^0\pi^+$ peak are allowed to vary in the fit to the data, whilst they are fixed for the very small $B^+ \rightarrow K_S^0 K^+$ peak contribution. The mean of the $B^+ \rightarrow K_S^0 K^+$ peak, around $5240 \text{ MeV}/c^2$, is fixed using the mass difference between the

Table 1: Summary of systematic uncertainties relative to the measured $B^+ \rightarrow p\bar{\Lambda}$ branching fraction. The contributions are split into those that come from the signal decay and those that come from the normalisation decay. The total corresponds to the sum of all contributions added in quadrature.

Source	Value [%]	
	$B^+ \rightarrow p\bar{\Lambda}$	$B^+ \rightarrow K_s^0\pi^+$
$\mathcal{B}(B^+ \rightarrow K_s^0\pi^+)$	-	3.2
Trigger efficiencies ratio	3.5	-
Selection efficiencies ratio	2.2	-
PID uncertainties	1.2	3.5
Tracking efficiencies ratio	6.0	-
Yields from mass fits	6.7	3.0
Simulation statistics	1.7	3.3
Total	10.1	6.5

$B^+ \rightarrow K_s^0K^+$ and $B^+ \rightarrow K_s^0\pi^+$ peaks obtained from simulation. The $B^+ \rightarrow K_s^0K^+$ yield is Gaussian constrained using the $B^+ \rightarrow K_s^0\pi^+$ yield, taking into account the differences in branching fraction and selection efficiency.

The partially reconstructed backgrounds that populate the lower-mass sideband are assumed to arise from the $B_{(s)}^0 \rightarrow K_s^0 h^+ h'^-$ decay modes with the largest branching fractions, namely $B^0 \rightarrow K_s^0\pi^+\pi^-$, $B^0 \rightarrow K_s^0K^+K^-$, $B_s^0 \rightarrow K_s^0\pi^+\pi^-$ and $B_s^0 \rightarrow K_s^0K^\pm\pi^\mp$ [27]. Only $B^0 \rightarrow K_s^0\pi^+\pi^-$, $B_s^0 \rightarrow K_s^0\pi^+\pi^-$ and $B_s^0 \rightarrow K_s^0K^\pm\pi^\mp$ are considered given that $B^0 \rightarrow K_s^0K^+K^-$ is further suppressed because of a low kaon-to-pion misidentification probability. The overall shape of the $B_{(s)}^0 \rightarrow K_s^0 h^+ h'^-$ decay modes in the $K_s^0\pi^+$ mass spectrum is obtained from simulation accounting for the relative yields related to different B -meson fragmentation probabilities, selection efficiencies and branching fractions. The invariant mass distribution of the combinatorial background is described by an exponential function, with the slope parameter determined from the mass fit.

The resulting spectrum shows a prominent $B^+ \rightarrow K_s^0\pi^+$ peak above little combinatorial and partially reconstructed background. The fit to the $K_s^0\pi^+$ spectrum, presented in Fig. 2, determines seven parameters: three shape parameters and four yields. The signal yield obtained is $N(B^+ \rightarrow K_s^0\pi^+) = 930 \pm 34$, where the uncertainty is statistical only.

5 Systematic uncertainties

The systematic uncertainties are reduced by performing the branching fraction measurement relative to a decay mode topologically identical to the decay of interest. Uncertainties arise from imperfect knowledge of the selection efficiencies, systematic uncertainties on the fitted yields, and uncertainties on the branching fractions of decays involved in the calculation of the $B^+ \rightarrow p\bar{\Lambda}$ branching fraction. The systematic uncertainties assigned to the measurement of the $B^+ \rightarrow p\bar{\Lambda}$ branching fraction are summarised in Table 1.

The uncertainty on the branching fraction of the normalisation channel,

$\mathcal{B}(B^+ \rightarrow K_s^0 \pi^+) = (11.895 \pm 0.375) \times 10^{-6}$ [28] (assuming that half of the K^0 mesons decay as a K_s^0), is taken as a systematic uncertainty. The uncertainties on the branching fractions $\mathcal{B}(\Lambda \rightarrow p\pi^-) = (63.9 \pm 0.5)\%$ and $\mathcal{B}(K_s^0 \rightarrow \pi^+\pi^-) = (69.20 \pm 0.05)\%$ are accounted for, but omitted from the table as they are negligible compared to all other sources of systematic uncertainty.

The determination of the selection efficiencies entails several sources of systematic uncertainty. A systematic uncertainty is assigned to take into account possible differences in the trigger efficiencies between data and simulation, following the procedure and studies described in Ref. [29]. The $B^+ \rightarrow K_s^0 \pi^+$ mode is used as a proxy for the assessment of the systematic uncertainties related to the MLP selection. Distributions for the $B^+ \rightarrow K_s^0 \pi^+$ MLP input variables are obtained from data using the *sPlot* technique. The distributions from simulation showing the largest discrepancies are weighted to match those of the data. The selection efficiencies are recalculated with the same MLPs, but using the weighted distributions, to derive the variations in efficiency, and hence the systematic uncertainty on the selection. The uncertainty associated with the imperfect knowledge of PID selection efficiencies is assessed varying the binning of the PID control samples in track momentum and pseudorapidity, and also accounting for a dependence of the efficiency on the event track multiplicity after weighting the distribution of the latter to match that of the data. The two uncertainties are combined in quadrature.

The signal decay has two baryons in the final state whilst only mesons are present in the final state of the normalisation channel. Tracking efficiency uncertainties do not cancel fully in this instance. The degree to which the simulation describes the hadronic interactions with the material is less accurate for baryons than it is for mesons. A systematic uncertainty of 4% per proton is estimated whereas the corresponding uncertainty is 1.5% for pions and kaons [30]. A non-negligible systematic uncertainty on the tracking efficiencies as calculated from simulation, including correlations, results from these sources of uncertainty.

Systematic uncertainties on the fit yields arise from potential mismodelling of the fit components and from the uncertainties on the values of the parameters fixed in the fits. They are investigated using data and by studying a large number of simulated data samples, with parameters varying within their estimated uncertainties. Changing the combinatorial background model to a linear shape decreases the signal yield by 4.6%, with no significant effect on the signal significance and the final result. Possible contamination from the unobserved decay $B^+ \rightarrow p\bar{\Sigma}^0$ is studied by adding such a component. The fitted $B^+ \rightarrow p\bar{\Sigma}^0$ yield is found to be compatible with zero, and the shift in the $B^+ \rightarrow p\bar{\Lambda}$ yield with respect to the nominal yield is taken as a systematic uncertainty.

The finite size of the simulation samples used in the analysis further contributes as a source of systematic uncertainty. The total systematic uncertainty on the $B^+ \rightarrow p\bar{\Lambda}$ branching fraction is given by the sum of all contributions added in quadrature, amounting to 12.0%.

6 Results and conclusion

The $B^+ \rightarrow p\bar{\Lambda}$ branching fraction is determined relative to that of the $B^+ \rightarrow K_s^0 \pi^+$ normalisation channel according to

$$\mathcal{B}(B^+ \rightarrow p\bar{\Lambda}) = \frac{N(B^+ \rightarrow p\bar{\Lambda})}{N(B^+ \rightarrow K_s^0 \pi^+)} \frac{\epsilon_{B^+ \rightarrow K_s^0 \pi^+}}{\epsilon_{B^+ \rightarrow p\bar{\Lambda}}} \frac{\mathcal{B}(K_s^0 \rightarrow \pi^+\pi^-)}{\mathcal{B}(\Lambda \rightarrow p\pi^-)} \mathcal{B}(B^+ \rightarrow K_s^0 \pi^+),$$

where N represent the yields determined from the mass fits and ϵ are the selection efficiencies. It is measured to be

$$\mathcal{B}(B^+ \rightarrow p\bar{\Lambda}) = (2.4_{-0.8}^{+1.0} \pm 0.3) \times 10^{-7},$$

where the first uncertainty is statistical and the second systematic.

In summary, a search is reported for the rare two-body charmless baryonic decay $B^+ \rightarrow p\bar{\Lambda}$ using a pp collision data sample collected by the LHCb experiment at centre-of-mass energies of 7 and 8 TeV, corresponding to an integrated luminosity of 3 fb^{-1} . An excess of $B^+ \rightarrow p\bar{\Lambda}$ candidates with respect to background expectations is found with a statistical significance of 4.1 standard deviations. This is the first evidence for this decay process.

The measured branching fraction is compatible with the theoretical predictions in Refs. [5,6] but is in tension with calculations based on QCD sum rules [4] and calculations based on factorisation with the hypothesis of the violation of partial conservation of the axial-vector current at the GeV scale [7]. It helps shed light on an area of hadronic physics in which experimental input is needed, namely the study of the mechanisms responsible for decays of B mesons to baryonic final states.

Acknowledgements

We express our gratitude to our colleagues in the CERN accelerator departments for the excellent performance of the LHC. We thank the technical and administrative staff at the LHCb institutes. We acknowledge support from CERN and from the national agencies: CAPES, CNPq, FAPERJ and FINEP (Brazil); NSFC (China); CNRS/IN2P3 (France); BMBF, DFG and MPG (Germany); INFN (Italy); FOM and NWO (The Netherlands); MNiSW and NCN (Poland); MEN/IFA (Romania); MinES and FASO (Russia); MinCo (Spain); SNSF and SER (Switzerland); NASU (Ukraine); STFC (United Kingdom); NSF (USA). We acknowledge the computing resources that are provided by CERN, IN2P3 (France), KIT and DESY (Germany), INFN (Italy), SURF (The Netherlands), PIC (Spain), GridPP (United Kingdom), RRCKI and Yandex LLC (Russia), CSCS (Switzerland), IFIN-HH (Romania), CBPF (Brazil), PL-GRID (Poland) and OSC (USA). We are indebted to the communities behind the multiple open source software packages on which we depend. Individual groups or members have received support from AvH Foundation (Germany), EPLANET, Marie Skłodowska-Curie Actions and ERC (European Union), Conseil Général de Haute-Savoie, Labex ENIGMASS and OCEVU, Région Auvergne (France), RFBR and Yandex LLC (Russia), GVA, XuntaGal and GENCAT (Spain), Herchel Smith Fund, The Royal Society, Royal Commission for the Exhibition of 1851 and the Leverhulme Trust (United Kingdom).

References

- [1] BaBar and Belle collaborations, A. J. Bevan *et al.*, *The physics of the B factories*, Eur. Phys. J. **C74** (2014) 3026, [arXiv:1406.6311](#).
- [2] LHCb collaboration, R. Aaij *et al.*, *Evidence for CP violation in $B^+ \rightarrow p\bar{p}K^+$ decays*, Phys. Rev. Lett. **113** (2014) 141801, [arXiv:1407.5907](#).

- [3] LHCb collaboration, R. Aaij *et al.*, *First evidence for the two-body charmless baryonic decay $B^0 \rightarrow p\bar{p}$* , JHEP **10** (2013) 005, arXiv:1308.0961.
- [4] V. L. Chernyak and I. R. Zhitnitsky, *B-meson exclusive decays into baryons*, Nucl. Phys. **B345** (1990) 137.
- [5] H.-Y. Cheng and K.-C. Yang, *Charmless exclusive baryonic B decays*, Phys. Rev. **D66** (2002) 014020, arXiv:hep-ph/0112245.
- [6] C.-K. Chua, *Charmless two-body baryonic $B_{u,d,s}$ decays revisited*, Phys. Rev. **D89** (2014) 056003, arXiv:1312.2335.
- [7] Y. K. Hsiao and C. Q. Geng, *Violation of partial conservation of the axial-vector current and two-body baryonic B and D_s decays*, Phys. Rev. **D91** (2015) 077501, arXiv:1407.7639.
- [8] CLEO collaboration, T. E. Coan *et al.*, *Search for exclusive rare baryonic decays of B mesons*, Phys. Rev. **D59** (1999) 111101, arXiv:hep-ex/9810043.
- [9] Belle collaboration, Y.-T. Tsai *et al.*, *Search for $B^0 \rightarrow p\bar{p}$, $\Lambda\bar{\Lambda}$ and $B^+ \rightarrow p\bar{\Lambda}$ at Belle*, Phys. Rev. **D75** (2007) 111101, arXiv:hep-ex/0703048.
- [10] LHCb collaboration, A. A. Alves Jr. *et al.*, *The LHCb detector at the LHC*, JINST **3** (2008) S08005.
- [11] LHCb collaboration, R. Aaij *et al.*, *LHCb detector performance*, Int. J. Mod. Phys. **A30** (2015) 1530022, arXiv:1412.6352.
- [12] V. V. Gligorov and M. Williams, *Efficient, reliable and fast high-level triggering using a bonsai boosted decision tree*, JINST **8** (2013) P02013, arXiv:1210.6861.
- [13] T. Sjöstrand, S. Mrenna, and P. Skands, *PYTHIA 6.4 physics and manual*, JHEP **05** (2006) 026, arXiv:hep-ph/0603175; T. Sjöstrand, S. Mrenna, and P. Skands, *A brief introduction to PYTHIA 8.1*, Comput. Phys. Commun. **178** (2008) 852, arXiv:0710.3820.
- [14] I. Belyaev *et al.*, *Handling of the generation of primary events in Gauss, the LHCb simulation framework*, J. Phys. Conf. Ser. **331** (2011) 032047.
- [15] D. J. Lange, *The EvtGen particle decay simulation package*, Nucl. Instrum. Meth. **A462** (2001) 152.
- [16] P. Golonka and Z. Was, *PHOTOS Monte Carlo: a precision tool for QED corrections in Z and W decays*, Eur. Phys. J. **C45** (2006) 97, arXiv:hep-ph/0506026.
- [17] Geant4 collaboration, J. Allison *et al.*, *Geant4 developments and applications*, IEEE Trans. Nucl. Sci. **53** (2006) 270; Geant4 collaboration, S. Agostinelli *et al.*, *Geant4 - a simulation toolkit*, Nucl. Instrum. Meth. **A506** (2003) 250.
- [18] M. Clemencic *et al.*, *The LHCb simulation application, Gauss: design, evolution and experience*, J. Phys. Conf. Ser. **331** (2011) 032023.

- [19] W. D. Hulsbergen, *Decay chain fitting with a Kalman filter*, Nucl. Instrum. Meth. **A552** (2005) 566, [arXiv:physics/0503191](#).
- [20] Particle Data Group, K. A. Olive *et al.*, *Review of particle physics*, Chin. Phys. **C38** (2014) 090001, and 2015 update.
- [21] D. E. Rumelhart, G. E. Hinton, and R. J. Williams, *Parallel distributed processing: explorations in the microstructure of cognition*, vol. 1, MIT, Cambridge, USA, 1986.
- [22] A. Hoecker *et al.*, *TMVA - toolkit for multivariate data analysis*, PoS **ACAT** (2007) 040, [arXiv:physics/0703039](#).
- [23] M. Pivk and F. R. Le Diberder, *sPlot: a statistical tool to unfold data distributions*, Nucl. Instrum. Meth. **A555** (2005) 356, [arXiv:physics/0402083](#).
- [24] G. Punzi, *Sensitivity of searches for new signals and its optimization*, in *Statistical Problems in Particle Physics, Astrophysics, and Cosmology* (L. Lyons, R. Mount, and R. Reitmeyer, eds.), p. 79, 2003. [arXiv:physics/0308063](#).
- [25] M. Adinolfi *et al.*, *Performance of the LHCb RICH detector at the LHC*, Eur. Phys. J. **C73** (2013) 2431, [arXiv:1211.6759](#).
- [26] T. Skwarnicki, *A study of the radiative cascade transitions between the Upsilon-prime and Upsilon resonances*, PhD thesis, Institute of Nuclear Physics, Krakow, 1986, DESY-F31-86-02.
- [27] LHCb collaboration, R. Aaij *et al.*, *Study of $B_{(s)}^0 \rightarrow K_S^0 h^+ h'^-$ decays with first observation of $B_s^0 \rightarrow K_S^0 K^\pm \pi^\mp$ and $B_s^0 \rightarrow K_S^0 \pi^+ \pi^-$* , JHEP **10** (2013) 143, [arXiv:1307.7648](#).
- [28] Heavy Flavor Averaging Group, Y. Amhis *et al.*, *Averages of b-hadron, c-hadron, and τ -lepton properties as of summer 2014*, [arXiv:1412.7515](#), updated results and plots available at <http://www.slac.stanford.edu/xorg/hfag/>.
- [29] LHCb collaboration, R. Aaij *et al.*, *Observation of the $\Lambda_b \rightarrow \Lambda \phi$ decay*, Phys. Lett. **B759** (2016) 282, [arXiv:1603.02870](#).
- [30] LHCb collaboration, R. Aaij *et al.*, *Measurement of the track reconstruction efficiency at LHCb*, JINST **10** (2015) P02007, [arXiv:1408.1251](#).

LHCb collaboration

R. Aaij⁴⁰, B. Adeva³⁹, M. Adinolfi⁴⁸, Z. Ajaltouni⁵, S. Akar⁶, J. Albrecht¹⁰, F. Alessio⁴⁰, M. Alexander⁵³, S. Ali⁴³, G. Alkhazov³¹, P. Alvarez Cartelle⁵⁵, A.A. Alves Jr⁵⁹, S. Amato², S. Amerio²³, Y. Amhis⁷, L. An⁴¹, L. Anderlini¹⁸, G. Andreassi⁴¹, M. Andreotti^{17,g}, J.E. Andrews⁶⁰, R.B. Appleby⁵⁶, F. Archilli⁴³, P. d'Argent¹², J. Arnau Romeu⁶, A. Artamonov³⁷, M. Artuso⁶¹, E. Aslanides⁶, G. Auriemma²⁶, M. Baalouch⁵, I. Babuschkin⁵⁶, S. Bachmann¹², J.J. Back⁵⁰, A. Badalov³⁸, C. Baesso⁶², S. Baker⁵⁵, W. Baldini¹⁷, R.J. Barlow⁵⁶, C. Barschel⁴⁰, S. Barsuk⁷, W. Barter⁴⁰, M. Baszczyk²⁷, V. Batozskaya²⁹, B. Batsukh⁶¹, V. Battista⁴¹, A. Bay⁴¹, L. Beaucourt⁴, J. Beddow⁵³, F. Bedeschi²⁴, I. Bediaga¹, L.J. Bel⁴³, V. Bellee⁴¹, N. Belloli^{21,i}, K. Belous³⁷, I. Belyaev³², E. Ben-Haim⁸, G. Bencivenni¹⁹, S. Benson⁴³, J. Benton⁴⁸, A. Berezhnoy³³, R. Bernet⁴², A. Bertolin²³, C. Betancourt⁴², F. Betti¹⁵, M.-O. Bettler⁴⁰, M. van Beuzekom⁴³, Ia. Bezshyiko⁴², S. Bifani⁴⁷, P. Billoir⁸, T. Bird⁵⁶, A. Birnkraut¹⁰, A. Bitadze⁵⁶, A. Bizzeti^{18,u}, T. Blake⁵⁰, F. Blanc⁴¹, J. Blouw^{11,†}, S. Blusk⁶¹, V. Bocci²⁶, T. Boettcher⁵⁸, A. Bondar^{36,w}, N. Bondar^{31,40}, W. Bonivento¹⁶, I. Bordyuzhin³², A. Borgheresi^{21,i}, S. Borghi⁵⁶, M. Borisyak³⁵, M. Borsato³⁹, F. Bossu⁷, M. Boubdir⁹, T.J.V. Bowcock⁵⁴, E. Bowen⁴², C. Bozzi^{17,40}, S. Braun¹², M. Britsch¹², T. Britton⁶¹, J. Brodzicka⁵⁶, E. Buchanan⁴⁸, C. Buri⁵⁶, A. Bursche², J. Buytaert⁴⁰, S. Cadeddu¹⁶, R. Calabrese^{17,g}, M. Calvi^{21,i}, M. Calvo Gomez^{38,m}, A. Camboni³⁸, P. Campana¹⁹, D.H. Campora Perez⁴⁰, L. Capriotti⁵⁶, A. Carbone^{15,e}, G. Carboni^{25,j}, R. Cardinale^{20,h}, A. Cardini¹⁶, P. Carniti^{21,i}, L. Carson⁵², K. Carvalho Akiba², G. Casse⁵⁴, L. Cassina^{21,i}, L. Castillo Garcia⁴¹, M. Cattaneo⁴⁰, Ch. Cauet¹⁰, G. Cavallero²⁰, R. Cenci^{24,t}, D. Chamont⁷, M. Charles⁸, Ph. Charpentier⁴⁰, G. Chatzikonstantinidis⁴⁷, M. Chefdeville⁴, S. Chen⁵⁶, S.-F. Cheung⁵⁷, V. Chobanova³⁹, M. Chrzaszcz^{42,27}, X. Cid Vidal³⁹, G. Ciezarek⁴³, P.E.L. Clarke⁵², M. Clemencic⁴⁰, H.V. Cliff⁴⁹, J. Closier⁴⁰, V. Coco⁵⁹, J. Cogan⁶, E. Cogneras⁵, V. Cogoni^{16,40,f}, L. Cojocariu³⁰, G. Collazuol^{23,o}, P. Collins⁴⁰, A. Comerma-Montells¹², A. Contu⁴⁰, A. Cook⁴⁸, G. Coombs⁴⁰, S. Coquereau³⁸, G. Corti⁴⁰, M. Corvo^{17,g}, C.M. Costa Sobral⁵⁰, B. Couturier⁴⁰, G.A. Cowan⁵², D.C. Craik⁵², A. Crocombe⁵⁰, M. Cruz Torres⁶², S. Cunliffe⁵⁵, R. Currie⁵⁵, C. D'Ambrosio⁴⁰, F. Da Cunha Marinho², E. Dall'Occo⁴³, J. Dalseno⁴⁸, P.N.Y. David⁴³, A. Davis⁵⁹, O. De Aguiar Francisco², K. De Bruyn⁶, S. De Capua⁵⁶, M. De Cian¹², J.M. De Miranda¹, L. De Paula², M. De Serio^{14,d}, P. De Simone¹⁹, C.-T. Dean⁵³, D. Decamp⁴, M. Deckenhoff¹⁰, L. Del Buono⁸, M. Demmer¹⁰, A. Dendek²⁸, D. Derkach³⁵, O. Deschamps⁵, F. Dettori⁴⁰, B. Dey²², A. Di Canto⁴⁰, H. Dijkstra⁴⁰, F. Dordei⁴⁰, M. Dorigo⁴¹, A. Dosil Suárez³⁹, A. Dovbnya⁴⁵, K. Dreimanis⁵⁴, L. Dufour⁴³, G. Dujany⁵⁶, K. Dungs⁴⁰, P. Durante⁴⁰, R. Dzhelyadin³⁷, A. Dziurda⁴⁰, A. Dzyuba³¹, N. Déléage⁴, S. Easo⁵¹, M. Ebert⁵², U. Egede⁵⁵, V. Egorychev³², S. Eidelman^{36,w}, S. Eisenhardt⁵², U. Eitschberger¹⁰, R. Ekelhof¹⁰, L. Eklund⁵³, S. Ely⁶¹, S. Esen¹², H.M. Evans⁴⁹, T. Evans⁵⁷, A. Falabella¹⁵, N. Farley⁴⁷, S. Farry⁵⁴, R. Fay⁵⁴, D. Fazzini^{21,i}, D. Ferguson⁵², A. Fernandez Prieto³⁹, F. Ferrari^{15,40}, F. Ferreira Rodrigues², M. Ferro-Luzzi⁴⁰, S. Filippov³⁴, R.A. Fini¹⁴, M. Fiore^{17,g}, M. Fiorini^{17,g}, M. Firlej²⁸, C. Fitzpatrick⁴¹, T. Fiutowski²⁸, F. Fleuret^{7,b}, K. Fohl⁴⁰, M. Fontana^{16,40}, F. Fontanelli^{20,h}, D.C. Forshaw⁶¹, R. Forty⁴⁰, V. Franco Lima⁵⁴, M. Frank⁴⁰, C. Frei⁴⁰, J. Fu^{22,q}, W. Funk⁴⁰, E. Furfaro^{25,j}, C. Färber⁴⁰, A. Gallas Torreira³⁹, D. Galli^{15,e}, S. Gallorini²³, S. Gambetta⁵², M. Gandelman², P. Gandini⁵⁷, Y. Gao³, L.M. Garcia Martin⁶⁹, J. García Pardiñas³⁹, J. Garra Tico⁴⁹, L. Garrido³⁸, P.J. Garsed⁴⁹, D. Gascon³⁸, C. Gaspar⁴⁰, L. Gavardi¹⁰, G. Gazzoni⁵, D. Gerick¹², E. Gersabeck¹², M. Gersabeck⁵⁶, T. Gershon⁵⁰, Ph. Ghez⁴, S. Giani⁴¹, V. Gibson⁴⁹, O.G. Girard⁴¹, L. Giubega³⁰, K. Gizdov⁵², V.V. Gligorov⁸, D. Golubkov³², A. Golutvin^{55,40}, A. Gomes^{1,a}, I.V. Gorelov³³, C. Gotti^{21,i}, M. Grabalosa Gándara⁵, R. Graciani Diaz³⁸, L.A. Granado Cardoso⁴⁰, E. Graugés³⁸, E. Graverini⁴², G. Graziani¹⁸, A. Greco³⁰, P. Griffith⁴⁷, L. Grillo^{21,40,i}, B.R. Gruberg Cazon⁵⁷, O. Grünberg⁶⁷, E. Gushchin³⁴, Yu. Guz³⁷, T. Gys⁴⁰,

C. Göbel⁶², T. Hadavizadeh⁵⁷, C. Hadjivasiliou⁵, G. Haefeli⁴¹, C. Haen⁴⁰, S.C. Haines⁴⁹,
 S. Hall⁵⁵, B. Hamilton⁶⁰, X. Han¹², S. Hansmann-Menzemer¹², N. Harnew⁵⁷, S.T. Harnew⁴⁸,
 J. Harrison⁵⁶, M. Hatch⁴⁰, J. He⁶³, T. Head⁴¹, A. Heister⁹, K. Hennessy⁵⁴, P. Henrard⁵,
 L. Henry⁸, E. van Herwijnen⁴⁰, M. Heß⁶⁷, A. Hicheur², D. Hill⁵⁷, C. Hombach⁵⁶, H. Hopchev⁴¹,
 W. Hulsbergen⁴³, T. Humair⁵⁵, M. Hushchyn³⁵, N. Hussain⁵⁷, D. Hutchcroft⁵⁴, M. Idzik²⁸,
 P. Ilten⁵⁸, R. Jacobsson⁴⁰, A. Jaeger¹², J. Jalocha⁵⁷, E. Jans⁴³, A. Jawahery⁶⁰, F. Jiang³,
 M. John⁵⁷, D. Johnson⁴⁰, C.R. Jones⁴⁹, C. Joram⁴⁰, B. Jost⁴⁰, N. Jurik⁵⁷, S. Kandybei⁴⁵,
 W. Kanso⁶, M. Karacson⁴⁰, J.M. Kariuki⁴⁸, S. Karodia⁵³, M. Kecke¹², M. Kelsey⁶¹,
 M. Kenzie⁴⁹, T. Ketel⁴⁴, E. Khairullin³⁵, B. Khanji¹², C. Khurewathanakul⁴¹, T. Kirn⁹,
 S. Klaver⁵⁶, K. Klimaszewski²⁹, S. Koliiev⁴⁶, M. Kolpin¹², I. Komarov⁴¹, R.F. Koopman⁴⁴,
 P. Koppenburg⁴³, A. Kosmyntseva³², A. Kozachuk³³, M. Kozeiha⁵, L. Kravchuk³⁴, K. Kreplin¹²,
 M. Kreps⁵⁰, P. Krokovny^{36,w}, F. Kruse¹⁰, W. Krzemien²⁹, W. Kucewicz^{27,l}, M. Kucharczyk²⁷,
 V. Kudryavtsev^{36,w}, A.K. Kuonen⁴¹, K. Kurek²⁹, T. Kvaratskheliya^{32,40}, D. Lacarrere⁴⁰,
 G. Lafferty⁵⁶, A. Lai¹⁶, G. Lanfranchi¹⁹, C. Langenbruch⁹, T. Latham⁵⁰, C. Lazzeroni⁴⁷,
 R. Le Gac⁶, J. van Leerdam⁴³, A. Leflat^{33,40}, J. Lefrançois⁷, R. Lefèvre⁵, F. Lemaitre⁴⁰,
 E. Lemos Cid³⁹, O. Leroy⁶, T. Lesiak²⁷, B. Leverington¹², T. Li³, Y. Li⁷, T. Likhomanenko^{35,68},
 R. Lindner⁴⁰, C. Linn⁴⁰, F. Lionetto⁴², X. Liu³, D. Loh⁵⁰, I. Longstaff⁵³, J.H. Lopes²,
 D. Lucchesi^{23,o}, M. Lucio Martinez³⁹, H. Luo⁵², A. Lupato²³, E. Luppi^{17,g}, O. Lupton⁵⁷,
 A. Lusiani²⁴, X. Lyu⁶³, F. Machefert⁷, F. Maciuc³⁰, O. Maev³¹, K. Maguire⁵⁶, S. Malde⁵⁷,
 A. Malinin⁶⁸, T. Maltsev³⁶, G. Manca⁷, G. Mancinelli⁶, P. Manning⁶¹, J. Maratas^{5,v},
 J.F. Marchand⁴, U. Marconi¹⁵, C. Marin Benito³⁸, P. Marino^{24,t}, J. Marks¹², G. Martellotti²⁶,
 M. Martin⁶, M. Martinelli⁴¹, D. Martinez Santos³⁹, F. Martinez Vidal⁶⁹, D. Martins Tostes²,
 L.M. Massacrier⁷, A. Massafferri¹, R. Matev⁴⁰, A. Mathad⁵⁰, Z. Mathe⁴⁰, C. Matteuzzi²¹,
 A. Mauri⁴², E. Maurice^{7,b}, B. Maurin⁴¹, A. Mazurov⁴⁷, M. McCann⁵⁵, J. McCarthy⁴⁷,
 A. McNab⁵⁶, R. McNulty¹³, B. Meadows⁵⁹, F. Meier¹⁰, M. Meissner¹², D. Melnychuk²⁹,
 M. Merk⁴³, A. Merli^{22,q}, E. Michielin²³, D.A. Milanes⁶⁶, M.-N. Minard⁴, D.S. Mitzel¹²,
 A. Mogini⁸, J. Molina Rodriguez¹, I.A. Monroy⁶⁶, S. Monteil⁵, M. Morandin²³, P. Morawski²⁸,
 A. Mordà⁶, M.J. Morello^{24,t}, J. Moron²⁸, A.B. Morris⁵², R. Mountain⁶¹, F. Muheim⁵²,
 M. Mulder⁴³, M. Mussini¹⁵, D. Müller⁵⁶, J. Müller¹⁰, K. Müller⁴², V. Müller¹⁰, P. Naik⁴⁸,
 T. Nakada⁴¹, R. Nandakumar⁵¹, A. Nandi⁵⁷, I. Nasteva², M. Needham⁵², N. Neri²²,
 S. Neubert¹², N. Neufeld⁴⁰, M. Neuner¹², T.D. Nguyen⁴¹, C. Nguyen-Mau^{41,n}, S. Nieswand⁹,
 R. Niet¹⁰, N. Nikitin³³, T. Nikodem¹², A. Novoselov³⁷, D.P. O'Hanlon⁵⁰,
 A. Oblakowska-Mucha²⁸, V. Obraztsov³⁷, S. Ogilvy¹⁹, R. Oldeman^{16,f}, C.J.G. Onderwater⁷⁰,
 J.M. Otalora Goicochea², A. Otto⁴⁰, P. Owen⁴², A. Oyanguren⁶⁹, P.R. Pais⁴¹, A. Palano^{14,d},
 F. Palombo^{22,q}, M. Palutan¹⁹, J. Panman⁴⁰, A. Papanestis⁵¹, M. Pappagallo^{14,d},
 L.L. Pappalardo^{17,g}, W. Parker⁶⁰, C. Parkes⁵⁶, G. Passaleva¹⁸, A. Pastore^{14,d}, G.D. Patel⁵⁴,
 M. Patel⁵⁵, C. Patrignani^{15,e}, A. Pearce^{56,51}, A. Pellegrino⁴³, G. Penso²⁶, M. Pepe Altarelli⁴⁰,
 S. Perazzini⁴⁰, P. Perret⁵, L. Pescatore⁴⁷, K. Petridis⁴⁸, A. Petrolini^{20,h}, A. Petrov⁶⁸,
 M. Petruzzo^{22,q}, E. Picatoste Olloqui³⁸, B. Pietrzyk⁴, M. Pikies²⁷, D. Pinci²⁶, A. Pistone²⁰,
 A. Piucci¹², V. Placinta³⁰, S. Playfer⁵², M. Plo Casasus³⁹, T. Poikela⁴⁰, F. Polci⁸,
 A. Poluektov^{50,36}, I. Polyakov⁶¹, E. Polcarpo², G.J. Pomery⁴⁸, A. Popov³⁷, D. Popov^{11,40},
 B. Popovici³⁰, S. Poslavskii³⁷, C. Potterat², E. Price⁴⁸, J.D. Price⁵⁴, J. Prisciandaro^{39,40},
 A. Pritchard⁵⁴, C. Prouve⁴⁸, V. Pugatch⁴⁶, A. Puig Navarro⁴², G. Punzi^{24,p}, W. Qian⁵⁷,
 R. Quagliani^{7,48}, B. Rachwal²⁷, J.H. Rademacker⁴⁸, M. Rama²⁴, M. Ramos Pernas³⁹,
 M.S. Rangel², I. Raniuk⁴⁵, F. Ratnikov³⁵, G. Raven⁴⁴, F. Redi⁵⁵, S. Reichert¹⁰, A.C. dos Reis¹,
 C. Remon Alepuz⁶⁹, V. Renaudin⁷, S. Ricciardi⁵¹, S. Richards⁴⁸, M. Rihl⁴⁰, K. Rinnert⁵⁴,
 V. Rives Molina³⁸, P. Robbe^{7,40}, A.B. Rodrigues¹, E. Rodrigues⁵⁹, J.A. Rodriguez Lopez⁶⁶,
 P. Rodriguez Perez^{56,†}, A. Rogozhnikov³⁵, S. Roiser⁴⁰, A. Rollings⁵⁷, V. Romanovskiy³⁷,
 A. Romero Vidal³⁹, J.W. Ronayne¹³, M. Rotondo¹⁹, M.S. Rudolph⁶¹, T. Ruf⁴⁰, P. Ruiz Valls⁶⁹,
 J.J. Saborido Silva³⁹, E. Sadykhov³², N. Sagidova³¹, B. Saitta^{16,f}, V. Salustino Guimaraes¹,

C. Sanchez Mayordomo⁶⁹, B. Sanmartin Sedes³⁹, R. Santacesaria²⁶, C. Santamarina Rios³⁹, M. Santimaria¹⁹, E. Santovetti^{25,j}, A. Sarti^{19,k}, C. Satriano^{26,s}, A. Satta²⁵, D.M. Saunders⁴⁸, D. Savrina^{32,33}, S. Schael⁹, M. Schellenberg¹⁰, M. Schiller⁵³, H. Schindler⁴⁰, M. Schlupp¹⁰, M. Schmelling¹¹, T. Schmelzer¹⁰, B. Schmidt⁴⁰, O. Schneider⁴¹, A. Schopper⁴⁰, K. Schubert¹⁰, M. Schubiger⁴¹, M.-H. Schune⁷, R. Schwemmer⁴⁰, B. Sciascia¹⁹, A. Sciubba^{26,k}, A. Semennikov³², A. Sergi⁴⁷, N. Serra⁴², J. Serrano⁶, L. Sestini²³, P. Seyfert²¹, M. Shapkin³⁷, I. Shapoval⁴⁵, Y. Shcheglov³¹, T. Shears⁵⁴, L. Shekhtman^{36,w}, V. Shevchenko⁶⁸, B.G. Siddi^{17,40}, R. Silva Coutinho⁴², L. Silva de Oliveira², G. Simi^{23,o}, S. Simone^{14,d}, M. Sirendi⁴⁹, N. Skidmore⁴⁸, T. Skwarnicki⁶¹, E. Smith⁵⁵, I.T. Smith⁵², J. Smith⁴⁹, M. Smith⁵⁵, H. Snoek⁴³, I. Soares Lavra¹, M.D. Sokoloff⁵⁹, F.J.P. Soler⁵³, B. Souza De Paula², B. Spaan¹⁰, P. Spradlin⁵³, S. Sridharan⁴⁰, F. Stagni⁴⁰, M. Stahl¹², S. Stahl⁴⁰, P. Stefko⁴¹, S. Stefkova⁵⁵, O. Steinkamp⁴², S. Stemmler¹², O. Stenyakin³⁷, S. Stevenson⁵⁷, S. Stoica³⁰, S. Stone⁶¹, B. Storaci⁴², S. Stracka^{24,p}, M. Straticiu³⁰, U. Straumann⁴², L. Sun⁶⁴, W. Sutcliffe⁵⁵, K. Swientek²⁸, V. Syropoulos⁴⁴, M. Szczekowski²⁹, T. Szumlak²⁸, S. T'Jampens⁴, A. Tayduganov⁶, T. Tekampe¹⁰, G. Tellarini^{17,g}, F. Teubert⁴⁰, E. Thomas⁴⁰, J. van Tilburg⁴³, M.J. Tilley⁵⁵, V. Tisserand⁴, M. Tobin⁴¹, S. Tolk⁴⁹, L. Tomassetti^{17,g}, D. Tonelli⁴⁰, S. Topp-Joergensen⁵⁷, F. Toriello⁶¹, E. Tournefier⁴, S. Tourneur⁴¹, K. Trabelsi⁴¹, M. Traill⁵³, M.T. Tran⁴¹, M. Tresch⁴², A. Trisovic⁴⁰, A. Tsaregorodtsev⁶, P. Tsopelas⁴³, A. Tully⁴⁹, N. Tuning⁴³, A. Ukleja²⁹, A. Ustyuzhanin³⁵, U. Uwer¹², C. Vacca^{16,f}, V. Vagnoni^{15,40}, A. Valassi⁴⁰, S. Valat⁴⁰, G. Valenti¹⁵, A. Vallier⁷, R. Vazquez Gomez¹⁹, P. Vazquez Regueiro³⁹, S. Vecchi¹⁷, M. van Veghel⁴³, J.J. Velthuis⁴⁸, M. Veltri^{18,r}, G. Veneziano⁵⁷, A. Venkateswaran⁶¹, M. Vernet⁵, M. Vesterinen¹², B. Viaud⁷, D. Vieira¹, M. Vieites Diaz³⁹, H. Viemann⁶⁷, X. Vilasis-Cardona^{38,m}, M. Vitti⁴⁹, V. Volkov³³, A. Vollhardt⁴², B. Voneki⁴⁰, A. Vorobyev³¹, V. Vorobyev^{36,w}, C. Voz⁶⁷, J.A. de Vries⁴³, C. Vázquez Sierra³⁹, R. Waldi⁶⁷, C. Wallace⁵⁰, R. Wallace¹³, J. Walsh²⁴, J. Wang⁶¹, D.R. Ward⁴⁹, H.M. Wark⁵⁴, N.K. Watson⁴⁷, D. Websdale⁵⁵, A. Weiden⁴², M. Whitehead⁴⁰, J. Wicht⁵⁰, G. Wilkinson^{57,40}, M. Wilkinson⁶¹, M. Williams⁴⁰, M.P. Williams⁴⁷, M. Williams⁵⁸, T. Williams⁴⁷, F.F. Wilson⁵¹, J. Wimberley⁶⁰, J. Wishahi¹⁰, W. Wislicki²⁹, M. Witek²⁷, G. Wormser⁷, S.A. Wotton⁴⁹, K. Wraight⁵³, K. Wyllie⁴⁰, Y. Xie⁶⁵, Z. Xing⁶¹, Z. Xu⁴¹, Z. Yang³, Y. Yao⁶¹, H. Yin⁶⁵, J. Yu⁶⁵, X. Yuan^{36,w}, O. Yushchenko³⁷, K.A. Zarebski⁴⁷, M. Zavertyaev^{11,c}, L. Zhang³, Y. Zhang⁷, Y. Zhang⁶³, A. Zhelezov¹², Y. Zheng⁶³, X. Zhu³, V. Zhukov⁹, S. Zucchelli¹⁵.

¹Centro Brasileiro de Pesquisas Físicas (CBPF), Rio de Janeiro, Brazil

²Universidade Federal do Rio de Janeiro (UFRJ), Rio de Janeiro, Brazil

³Center for High Energy Physics, Tsinghua University, Beijing, China

⁴LAPP, Université Savoie Mont-Blanc, CNRS/IN2P3, Annecy-Le-Vieux, France

⁵Clermont Université, Université Blaise Pascal, CNRS/IN2P3, LPC, Clermont-Ferrand, France

⁶CPPM, Aix-Marseille Université, CNRS/IN2P3, Marseille, France

⁷LAL, Université Paris-Sud, CNRS/IN2P3, Orsay, France

⁸LPNHE, Université Pierre et Marie Curie, Université Paris Diderot, CNRS/IN2P3, Paris, France

⁹I. Physikalisches Institut, RWTH Aachen University, Aachen, Germany

¹⁰Fakultät Physik, Technische Universität Dortmund, Dortmund, Germany

¹¹Max-Planck-Institut für Kernphysik (MPIK), Heidelberg, Germany

¹²Physikalisches Institut, Ruprecht-Karls-Universität Heidelberg, Heidelberg, Germany

¹³School of Physics, University College Dublin, Dublin, Ireland

¹⁴Sezione INFN di Bari, Bari, Italy

¹⁵Sezione INFN di Bologna, Bologna, Italy

¹⁶Sezione INFN di Cagliari, Cagliari, Italy

¹⁷Sezione INFN di Ferrara, Ferrara, Italy

¹⁸Sezione INFN di Firenze, Firenze, Italy

¹⁹Laboratori Nazionali dell'INFN di Frascati, Frascati, Italy

²⁰Sezione INFN di Genova, Genova, Italy

²¹Sezione INFN di Milano Bicocca, Milano, Italy

- ²² *Sezione INFN di Milano, Milano, Italy*
- ²³ *Sezione INFN di Padova, Padova, Italy*
- ²⁴ *Sezione INFN di Pisa, Pisa, Italy*
- ²⁵ *Sezione INFN di Roma Tor Vergata, Roma, Italy*
- ²⁶ *Sezione INFN di Roma La Sapienza, Roma, Italy*
- ²⁷ *Henryk Niewodniczanski Institute of Nuclear Physics Polish Academy of Sciences, Kraków, Poland*
- ²⁸ *AGH - University of Science and Technology, Faculty of Physics and Applied Computer Science, Kraków, Poland*
- ²⁹ *National Center for Nuclear Research (NCBJ), Warsaw, Poland*
- ³⁰ *Horia Hulubei National Institute of Physics and Nuclear Engineering, Bucharest-Magurele, Romania*
- ³¹ *Petersburg Nuclear Physics Institute (PNPI), Gatchina, Russia*
- ³² *Institute of Theoretical and Experimental Physics (ITEP), Moscow, Russia*
- ³³ *Institute of Nuclear Physics, Moscow State University (SINP MSU), Moscow, Russia*
- ³⁴ *Institute for Nuclear Research of the Russian Academy of Sciences (INR RAN), Moscow, Russia*
- ³⁵ *Yandex School of Data Analysis, Moscow, Russia*
- ³⁶ *Budker Institute of Nuclear Physics (SB RAS), Novosibirsk, Russia*
- ³⁷ *Institute for High Energy Physics (IHEP), Protvino, Russia*
- ³⁸ *ICCUB, Universitat de Barcelona, Barcelona, Spain*
- ³⁹ *Universidad de Santiago de Compostela, Santiago de Compostela, Spain*
- ⁴⁰ *European Organization for Nuclear Research (CERN), Geneva, Switzerland*
- ⁴¹ *Ecole Polytechnique Fédérale de Lausanne (EPFL), Lausanne, Switzerland*
- ⁴² *Physik-Institut, Universität Zürich, Zürich, Switzerland*
- ⁴³ *Nikhef National Institute for Subatomic Physics, Amsterdam, The Netherlands*
- ⁴⁴ *Nikhef National Institute for Subatomic Physics and VU University Amsterdam, Amsterdam, The Netherlands*
- ⁴⁵ *NSC Kharkiv Institute of Physics and Technology (NSC KIPT), Kharkiv, Ukraine*
- ⁴⁶ *Institute for Nuclear Research of the National Academy of Sciences (KINR), Kyiv, Ukraine*
- ⁴⁷ *University of Birmingham, Birmingham, United Kingdom*
- ⁴⁸ *H.H. Wills Physics Laboratory, University of Bristol, Bristol, United Kingdom*
- ⁴⁹ *Cavendish Laboratory, University of Cambridge, Cambridge, United Kingdom*
- ⁵⁰ *Department of Physics, University of Warwick, Coventry, United Kingdom*
- ⁵¹ *STFC Rutherford Appleton Laboratory, Didcot, United Kingdom*
- ⁵² *School of Physics and Astronomy, University of Edinburgh, Edinburgh, United Kingdom*
- ⁵³ *School of Physics and Astronomy, University of Glasgow, Glasgow, United Kingdom*
- ⁵⁴ *Oliver Lodge Laboratory, University of Liverpool, Liverpool, United Kingdom*
- ⁵⁵ *Imperial College London, London, United Kingdom*
- ⁵⁶ *School of Physics and Astronomy, University of Manchester, Manchester, United Kingdom*
- ⁵⁷ *Department of Physics, University of Oxford, Oxford, United Kingdom*
- ⁵⁸ *Massachusetts Institute of Technology, Cambridge, MA, United States*
- ⁵⁹ *University of Cincinnati, Cincinnati, OH, United States*
- ⁶⁰ *University of Maryland, College Park, MD, United States*
- ⁶¹ *Syracuse University, Syracuse, NY, United States*
- ⁶² *Pontifícia Universidade Católica do Rio de Janeiro (PUC-Rio), Rio de Janeiro, Brazil, associated to ²*
- ⁶³ *University of Chinese Academy of Sciences, Beijing, China, associated to ³*
- ⁶⁴ *School of Physics and Technology, Wuhan University, Wuhan, China, associated to ³*
- ⁶⁵ *Institute of Particle Physics, Central China Normal University, Wuhan, Hubei, China, associated to ³*
- ⁶⁶ *Departamento de Física, Universidad Nacional de Colombia, Bogota, Colombia, associated to ⁸*
- ⁶⁷ *Institut für Physik, Universität Rostock, Rostock, Germany, associated to ¹²*
- ⁶⁸ *National Research Centre Kurchatov Institute, Moscow, Russia, associated to ³²*
- ⁶⁹ *Instituto de Física Corpuscular (IFIC), Universitat de Valencia-CSIC, Valencia, Spain, associated to ³⁸*
- ⁷⁰ *Van Swinderen Institute, University of Groningen, Groningen, The Netherlands, associated to ⁴³*
- ^a *Universidade Federal do Triângulo Mineiro (UFTM), Uberaba-MG, Brazil*
- ^b *Laboratoire Leprince-Ringuet, Palaiseau, France*
- ^c *P.N. Lebedev Physical Institute, Russian Academy of Science (LPI RAS), Moscow, Russia*
- ^d *Università di Bari, Bari, Italy*
- ^e *Università di Bologna, Bologna, Italy*

^f *Università di Cagliari, Cagliari, Italy*

^g *Università di Ferrara, Ferrara, Italy*

^h *Università di Genova, Genova, Italy*

ⁱ *Università di Milano Bicocca, Milano, Italy*

^j *Università di Roma Tor Vergata, Roma, Italy*

^k *Università di Roma La Sapienza, Roma, Italy*

^l *AGH - University of Science and Technology, Faculty of Computer Science, Electronics and Telecommunications, Kraków, Poland*

^m *LIFAEELS, La Salle, Universitat Ramon Llull, Barcelona, Spain*

ⁿ *Hanoi University of Science, Hanoi, Viet Nam*

^o *Università di Padova, Padova, Italy*

^p *Università di Pisa, Pisa, Italy*

^q *Università degli Studi di Milano, Milano, Italy*

^r *Università di Urbino, Urbino, Italy*

^s *Università della Basilicata, Potenza, Italy*

^t *Scuola Normale Superiore, Pisa, Italy*

^u *Università di Modena e Reggio Emilia, Modena, Italy*

^v *Iligan Institute of Technology (IIT), Iligan, Philippines*

^w *Novosibirsk State University, Novosibirsk, Russia*

[†] *Deceased*